# Design, Prototyping, and Characterization of Laser-Induced Graphene (LIG) Antennas on Flexible Substrates

**Alessio Mostaccio,** ***Graduate Student Member, IEEE,*** **Gaetano Marrocco,** ***Senior Member, IEEE***

*Pervasive Electromagnetics Lab, University of Rome Tor Vergata, Via del Politecnico 1, Rome, Italy (e-mail: alessio.mostaccio@uniroma2.it, gaetano.marrocco@uniroma2.it)*

Manuscript received March 3, 2008; revised November 10, 2008. First published December 10, 2008. Current version published February 25, 2009. Work partly funded by European Union - NextGenerationEU, ECS 0000024 Rome Technopole, CUP B83C22002820006, PNRR Mission 4, Component 2, Investment 1.5.

**Abstract:** Laser induction of graphene (LIG) is a widespread technology for the manufacturing of low-cost and eco-friendly sensors that can be also exploited for the fabrication of conductor-less antennas and radiofrequency devices for the personal and industrial Internet of Things.

In this case, additional issues must be accounted for, such as the much larger lasing area, the moderate conductivity of LIG, the durability versus environmental and mechanical conditions in real applications, but also new opportunities to provide antennas with non-conventional features. This paper provides a unitary representation of the state of the art knowledge for the modeling, design, fabrication, and test of LIG-based antennas at some frequencies of IoT systems.

The reader will find information about the selection of materials, on how to configure the laser parameters to minimize the sheet resistance, and how to account for the moderate conductivity in numerical solvers. The upper-bound performances are identified and related to the optimal antenna size. As IoT devices include sensors, the integration with the antenna can benefit from non-uniform lasing to dump unwanted RF currents on the sensor while preserving the communication capability. Finally, the immunity of LIG antennas to external stimuli is reviewed to quantify the expected degradation of performance. This tutorial hence provides a multi-disciplinary background to activate a new research line as well as to make experiments with the new concept of antennas engraved on substrates.

**Index Terms:** Laser-Induced Graphene (LIG), IoT, Flexible, Antenna, Sensor, RFID

## 1. Introduction

LASER induction is a fast, easy, and low-cost manufacturing technique for obtaining graphene traces starting from a high-carbon-content precursor substrate [1]. The technique, indeed, simply relies on an infrared laser inducing a photo-thermal effect in the material to remove all the atoms other than carbon. The so-obtained graphene, namely Laser-Induced Graphene (LIG), was extensively studied in the last decade for the manufacturing of graphene-based sensors: strain/bending transducers have been proposed in [2]–[5], pressure was evaluated in [6]–[8], but also gas concentration [9], [10], as well as temperature and RH [11]–[14] information were successfully retrieved by means of LIG. Furthermore, other common LIG applications concern supercapacitors [15], [16], electrodes and triboelectric nanogenerators [17]. Most of the above devices work at low frequencies, a few kHz at most, and rely on the connection to a data sampling unit.

Very recently, LIG potentialities have been investigated for manufacturing antennas working at higher frequencies (MHz and even GHz). The first LIG antenna, presented in 2020, was a coplanar waveguide (CPW) monopole resonating at $5.8$ GHz, manufactured starting from Poly-Ether-Sulfone (PES) as a precursor [18]. The same technology was then applied for patch antennas [19]–[21] and even for Radio Frequency

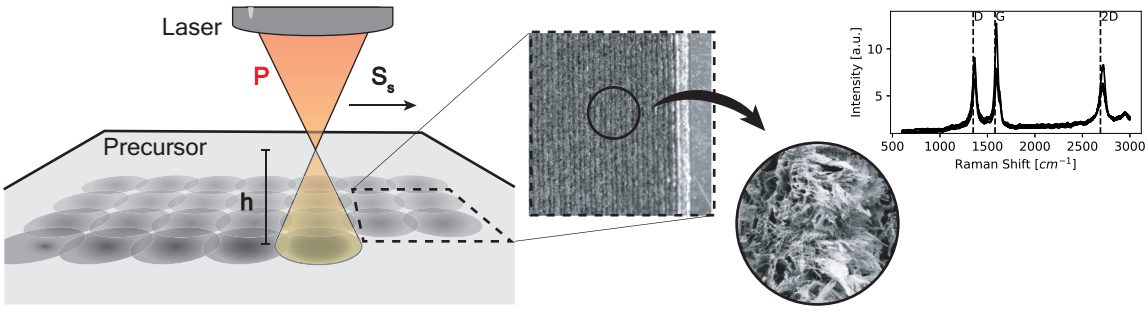


Fig. 1: (a) Sketch of the lasing process and of the laser parameters affecting it. (b) - (c) Magnification of LIG traces achieved by means of stereomicroscopy and Scanning Electron Microscopy (SEM). (d) Example of Raman spectra for LIG samples.

IDentification (RFID) tags [22]–[25]. The reported antennas show in some cases notable performances thanks to the working frequency in the micro and millimeter wave region and/or the presence of a metallic ground plane [18], [19], [21], [26]. In the case of full-LIG antennas, instead, the radiation gain significantly decreases ($-12/-8$ dBi) with a loss of performance w.r.t. metallic counterpart ranging from $10$ times or at least to $4$ times in the case of optimization of the layout.

Antennas exhibit distinctive characteristics when compared to sensors or electrodes made by LIG, and first of all the much larger size (square centimeters vs, square millimeters) and the high impact of the sheet resistance on the main radiation performance. A sheet resistance of tens of ohm/square ($\Omega/sq.$) that could be acceptable for interdigital capacitors working at a few kHz, would instead return a very poor radiation efficiency in the case of a dipole antenna, making it unusable. The limited conductivity of LIG significantly increases the input resistance of the antenna, making the matching to low impedance (as in the case of electromagnetic labels) much more challenging than for copper-based conductors. The lasing of a large area is expected to produce surface deformation due to thermal bending. Simultaneously, the lasing patterning, which is negligible in the case of small surfaces, can instead induce preferential currents paths [28], and hence anisotropy of the sheet resistance on antennas. Moreover, the antenna footprint, typically comparable to a wavelength, leads to several issues: i) antennas are prone to bending with a small curvature radius when affixed to objects or human skin; ii) they are commonly exposed to unpredictable environmental conditions in real-world applications, including variable temperature and humidity; iii) they may undergo mechanical stress, such as contact with hard objects, exerting pressure on the LIG surface; and, iv) they may come into contact with wet materials, such as skin or food and vegetables, releasing water moisture. All of these phenomena are expected to induce temporary or permanent modifications to the intimate structure of LIG.

Nevertheless, the many parameters of the lasing process may offer uncommon possibilities in antenna manufacturing and in particular the fabrication of non-uniform engineered conducting surfaces. Accordingly, the design of an efficient and reliable antenna by LIG techniques has to comprehensively address a set of electrical and physical constraints and options for a reliable application in real life.

This paper represents a first comprehensive effort to consolidate current knowledge on the design, fabrication and optimization of LIG antennas. The resume starts with a detailed examination of material selection and laser engraving parameters (Section II). Then, the paper delves into numerical modeling and the estimation of upper-bound radiation performance (Section III), considering topics related to manufacturing processes and different frequency ranges. The integration with complementary components and the fine-tuning of heterostructures are thoroughly discussed in Section IV. The investigation extends to the evaluation of performance and durability under real-world conditions in Section V. This synthesis offers a valuable compilation of essential insights, drawn partly from recent scientific literature and primarily from the direct expertise of the authors. It aims at providing the necessary knowledge to swiftly initiate new research endeavors in this field and facilitate experiments with application-oriented designs.

## 2. Materials & Fabrication

### 2.1. Precursors

Any carbon based material containing aromatic rings within its structure could be used as precursor substrate for LIG process [29]. Thermoplastic polymers, such as PolyImide (PI) and Poly-ether-Imide (PEI) [30], Kevlar [31], [32], Poly-ether-ether-ketone (PEEK) [33], [34], poly-ether-sulfone (PES) [35], [36], have a natural capability to withstand high temperatures. Temperature-sensitive materials (e.g. paper [5], wood [37]–[39], cloths, food [29], [40] silk [41]) can be converted into LIG as well but after a pre-treatment with flame retardants to prevent ablation and volatilization in ambient air [42].

This work only focuses on PI-derived LIG since it is widespread thanks to its excellent chemical, thermal, and electrical properties, it has the highest content of carbon within its structure [54], and it does not require any pre-treatment with flame retardant solutions which would be otherwise incompatible with some of the intended applications. Different types of PI, and thus of manufacturers, may differ in terms of carbon content and thus in the quality of the achieved LIG. We will particularly refer to the PI sheets as in [55], [56]. It is worth noting that different types of precursor as well as of laser cutter lead to significant differences in terms of chemical and electrical properties. Accordingly, a preliminary characterization task aimed at selecting the most appropriate set of parameters for the considered setup must be completed to feed the numerical model used for the antenna design.

### 2.2. Lasing Process

The conversion of the precursor into LIG relies on a photothermal effect [1], [57]–[59]. The emitted photons, indeed, are not powerful enough to directly break the covalent bonds between carbon and other atoms, but they induce an increment of temperature ($> 2500\ ^\circ C$) that makes the atomic structure of the precursor vibrating. At this stage, the bonds are indirectly broken with a rearrangement of carbon hybridization from the existing $sp^3$ to the $sp^2$ state thus producing an increment of conductivity.

Despite IR $CO_2$ lasers being the most common choice for the laser induction of graphene, the latter can be achieved also by means of UV lasers that grant resolutions $10$ times better (i.e., $5 - 10\ \mu m$) than the IR case. Differently from before, here, the incident photons directly break the covalent bonds thanks to the shorter wavelength ($< 400\ nm$) and thus to the higher energy they carry [58].

The features of the obtained graphene, i.e., the density of defects within its atomic structure, the macroscopic morphology, the electrical properties, and the chemical ones are strongly dependent on the lasing conditions [60], [61]. The irradiation is controlled mainly by the laser power ($P$), the scan speed ($S_s$), and the spot's size, which can be varied by means of a vertical offset ($h$) of the laser's head thus defocusing the beam [42] (Fig. 1a). Laser power is the most impacting parameter since it determines the amount of precursor converted into graphene; hence, as a rule of thumb, the higher the power, the higher the resulting conductivity [43], [62]. The beam cross-section enforces the overlapping among adjacent spots thus granting a more homogeneous conductor and a lower sheet resistance [29], [61]. The beam cross-section is controlled by the defocusing parameter: a beam with a large cross-section makes the process more sensitive to wrinkles and/or misalignment of the substrate that may lead to an uneven focal plane. Finally, second-order parameters, such as the carbon content of the precursor and its thickness [30], the density (DPI) of the layout image to engrave [45] or the environmental conditions [63] can affect the quality of the achieved LIG. Thicker substrates can withstand higher laser power, allowing a greater amount of precursor to be converted into LIG without undergoing ablation. Thus, we expect possible improvement by combining inkjet printed substrates made by thermoplastic polymers, such as PEEK (Poly Ether Ether Ketone), PES (Poly-Ether-Sulfone), PSU (Poly-Sulfone), and PP (Poly-Propylene) with laser engraving. DPI parameter (*dots-per-inch*), differently from defocusing, sets the resolution of the image and thus the number of spots within the same area without modifying their size. Inert atmospheres, such as Ar or $N_2$ ones, influence the chemical (e.g. the water contact angle) and electrical properties [29], [63] leading to a better quality graphene.

Fig. 1b and 1c show an example of LIG morphology obtained by means of the Speedy 100 laser cutter by Trotec. Stereomicroscopy and Scanning Electron Microscopy (SEM) are fundamental to investigate the macroscopic and microscopic morphology of LIG, respectively, while Raman analysis (Fig. 1d) reveals the atomic structure of the achieved graphene. As a matter of fact, the ratio between peaks $I_D/I_G$ in the Raman spectra returns the quality of the achieved LIG being proportional to the number of defects within the structure; while $I_{2D}/I_G$ determines the number of graphene's layers (the closer to $1$, the closer the material to a single layer graphene sheet) [62], [64].

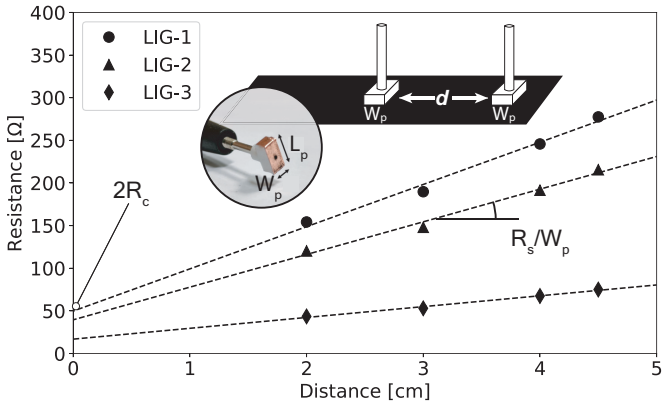


Fig. 2: Example of measured two-point resistance of LIG different stripes ($5$ cm x $1$ cm) w.r.t. the distance between the probes. The dashed lines are the LSQ regressions for each dataset.

TABLE I: LASER SETTINGS EMPLOYED FOR LIG SAMPLES

| Configuration | P [W] | $S_s$ [cm/s] | h [mm] | $I_D/I_G$ | $I_{2D}/I_G$ | $R_s$ [$\Omega/sq.$] | $R_C$ [$\Omega$] |
|---|---|---|---|---|---|---|---|
| **LIG-1** | 3.5 | 4.2 | 0 | $0.94 \pm 0.07$ | $0.63 \pm 0.10$ | $43.7 \pm 0.33$ | $18.2 \pm 0.3$ |
| **LIG-2** | 9 | 10 | 0 | $1.04 \pm 0.06$ | $0.62 \pm 0.01$ | $33.4 \pm 0.33$ | $16.6 \pm 0.3$ |
| **LIG-3** | 9 | 10 | 3 | $0.99 \pm 0.13$ | $0.84 \pm 0.11$ | $12.3 \pm 0.31$ | $6.1 \pm 0.3$ |

### *2.3. Electrical Characterization*

The electrical features of LIG devices are characterized by the sheet resistance $R_S$ [65], the contact resistance $R_C$ and the sheet inductance $L_S$, whose value, in case of graphene, is higher than that of standard conductors [66], [67].

#### 2.3.1. Sheet and Contact Resistances

The sheet resistance of graphene is practically frequency-independent up to tens of GHz [68]. The cut-off frequency depends on the doping level, the temperature, and the presence of defects [68], [69]. The contact resistance is the resistance due to the contact between the material and the metallic connector/probe/lumped electronic component [70]. The above resistances can be evaluated in DC by means of the Transfer Length Method (TLM) [71] that permits to decouple the two contributions. It involves measuring a two-point resistance of a LIG strip while gradually increasing the distance (*d*) between the probes [60], [62]. Then, by means of the Least Squares method, a linear regression is enforced on the measured data as $R = (R_s/W_p)\, d + 2R_c$. Accordingly, the $R_S$ is estimated as the slope of the regression line, multiplied by the width of the measuring pad. The contact resistance is equal to one-half the intercept with the y-axis. Fig. 2 shows examples of measured profiles of resistance for three laser settings reported in Tab. I. The LIG-3 configuration, which corresponds to the highest power and beam defocusing, exhibits the lowest sheet resistance ($R_S \approxeq 12\ \Omega/sq.$) and hence is the best suited for antenna fabrication. LIG-1 configuration, instead, could be used as an absorber.

This capability to modulate the feature of the LIG by changing the laser settings is the foundation for the design and manufacturing of heterostructures combining antennas and sensors.

#### 2.3.2. Sheet Inductance

Sheet inductance estimation must be performed in the frequency band of interest. Furthermore, since sheet inductance is expected to be of the order of hundreds of $pH/sq.$ for multilayer graphene sheets [66], [72], [73], non contacting measurement methods should be preferred to avoid artifacts due to the connection fixtures. The most assessed measurement techniques are *(i)* the waveguide method [73]–[76], *(ii)* the resonant cavity method [72], [77], and *(iii)* the microstrip resonators [78], [79]. In all the cases, a de-embedding procedure is required to remove artifacts.

Below $1$ GHz, the surface inductance ($pH/sq.$) can be considered negligible [72].

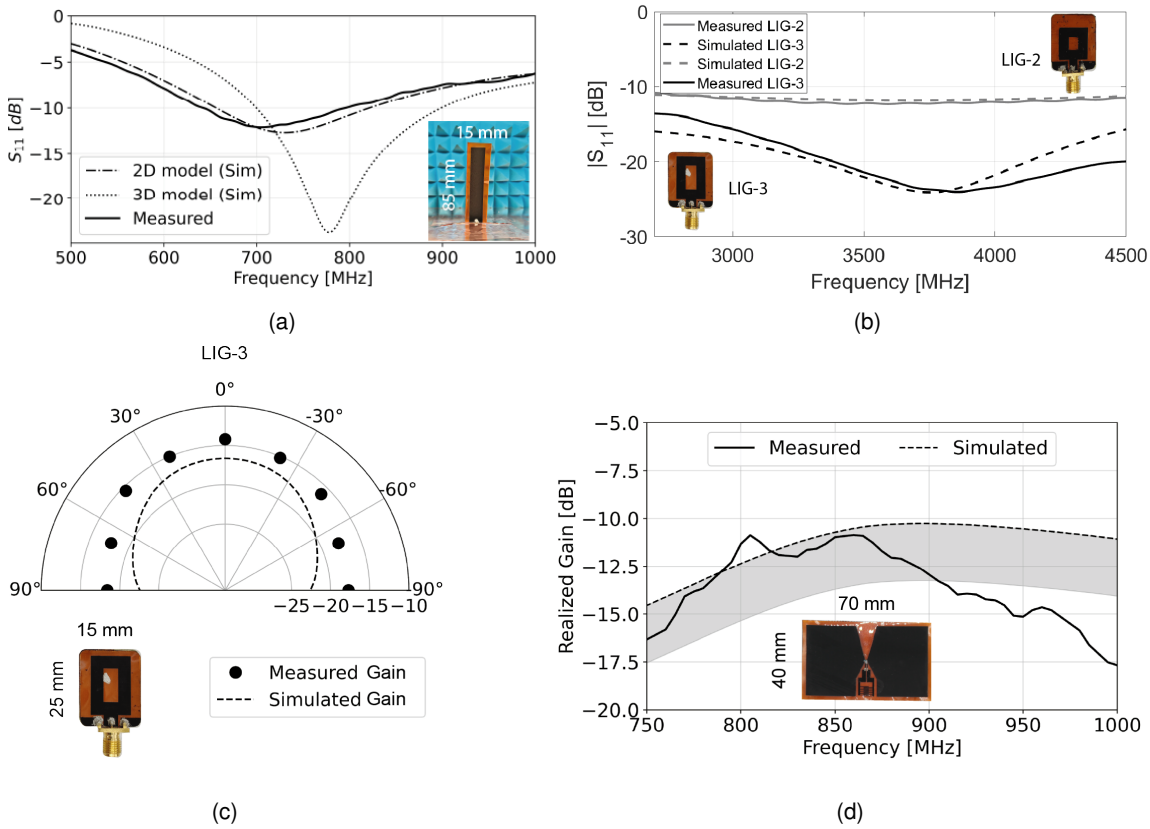


Fig. 3: Numerical simulations of LIG antennas by the FDTD method, and comparison with measurements: (a) reflection coefficient of a $L = 85$ mm by $W = 15$ mm rectangular monopole made by LIG-3 ($R_S$=12 $\Omega/sq.$) on a copper ground plane resonating in the UHF band, (b) reflection coefficient of a ring monopole ($L = 25$ mm, $W = 15$ mm) resonating at $3600$ MHz for LIG-2 and LIG-3. (c) Radiation pattern of the above monopole (LIG-3). (d) Simulated and measured realized gain of a $70 \times 40\ mm^2$ rectangular dipole with an integrated capacitive sensor.

## 3. Numerical Modeling and Upperbound Radiation Performance

### 3.1. Numerical Modeling

Graphene fabricated by lasing can be considered as a thin semi-conductor with a sheet resistance generally of the order of $1 - 10\ \Omega/sq.$ in best cases. Hence, the skin depth is approximately two orders of magnitude larger than the typical thickness of traces, i.e. from few to tens of micrometers [80]. Accordingly, LIG traces must be accounted for through a 2D model exploiting the Leontovich's condition, which relies on a complex-valued surface impedance (1)

$$\underline{E}_t = Z_s \underline{H}_t \times \hat{n} \tag{1}$$

where $\hat{n}$ is the normal unitary vector of the LIG trace and

$$Z_s = R_s + j\omega L_s \tag{2}$$

is the surface impedance for the graphene [72]. Fig. 3 shows some examples of simulations of planar dipoles and monopoles made of LIG of different settings (low and high sheet resistances) in comparison with simulations by the Finite Difference Time Domain (FDTD) method in the CST Studio 2023 implementation. Both input parameters and radiation gain are reported at different frequencies. In all cases, the Leontovich condition provides a good matching with real data both in terms of the resonant frequency and of the radiation efficiency. It is worth warning that other potential modeling options such as i) a 3D conductor with a uniform value of conductivity or ii) a high-loss 3D dielectric, would have been unpractical. Indeed, we experienced that the first one would have returned completely wrong results (Fig. 3a), while the second model would

TABLE II: UPPERBOUND RADIATION EFFICIENCY AND OPTIMAL SIZE OF LIG DIPOLES

| LIG | Frequency [MHz] | $\mathbf{L}/\lambda$ | $\mathbf{W}/\lambda$ | $\eta_{\mathbf{R,max}}$ [-] ($\mathbf{G_{max}}$ [dBi]) |
|---|---|---|---|---|
| **2** | 868 | 0.6 | 0.06 | 0.31 (−5.1) |
| | 2400 | 0.8 | 0.06 | 0.36 (−4.44) |
| | 3600 | 0.6 | 0.06 | 0.32 (−4.9) |
| **3** | 868 | 0.6 | 0.06 | 0.63 (−2.0) |
| | 2400 | 0.8 | 0.06 | 0.65 (−1.9) |
| | 3600 | 0.6 | 0.06 | 0.62 (−2.1) |

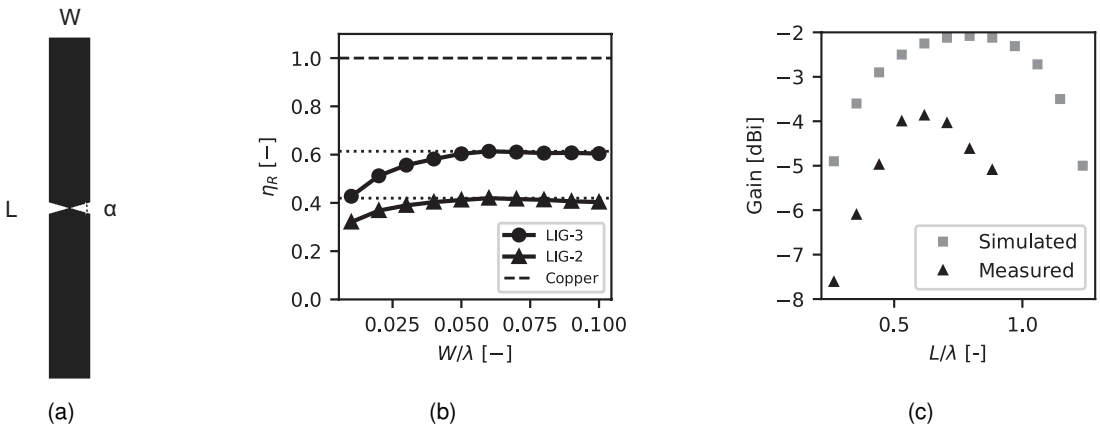


(a) (b) (c)

Fig. 4: Parametric analysis of a $L \times W$ rectangular dipole antenna. (a) Antenna layout on a Polyimide sheet. (b) Variation of radiation efficiency w.r.t to $W/\lambda$ for $L/\lambda = 0.6$ (c) Numerical and experimental results for a $R_S = 12\ \Omega/sq.$ dipole of size $W = 15$ mm.

have required a highly fine mesh of the graphene thickness producing long computation times and numerical instabilities.

### *3.2. Optimal size vs. frequency and $R_s$*

The radiation efficiency and gains of an antenna made by a high-loss conductor, as in the case of LIGs, is a non-monotonic function of the antenna size [81]. Indeed, the radiation resistance generally increases along with the enlargement of the antenna size, as well as the loss resistance. Since these two competing phenomena obey different laws, there exists an upper bound performance of the radiation efficiency and an optimal antenna size, that can be considered a reference value for designers. For example, Tab. II shows the maximum radiation efficiency and corresponding size at three typical IoT frequencies {868 MHz, 2400 MHz, and 3600 MHz}, of a $L \times W$ rectangular dipole for two values of sheet resistances $R_S = \{33,\ 12\}[\Omega/sq.]$ corresponding to laser settings LIG-2 and LIG-3 of Tab. I. It is worth noting that the maximum achievable radiation efficiency, as well as the optimal size, are frequency-independent. The upper bound efficiency is roughly 35% and 65% for the higher and lower considered sheet resistances, respectively, and correspond to a degradation of 4.5 dB and 2 dB w.r.t to a copper dipole of comparable size. The upper bound efficiency is roughly 35% and 65% for the considered high and low sheet resistances, respectively, and correspond to a degradation of 4.5 dB and 2 dB w.r.t to a copper dipole of comparable size. For both cases, the optimal lengths of LIG dipoles are $0.6 < L/\lambda < 0.8$, respectively. The efficiency can be partly improved by widening the width of the antenna trace. Indeed, from (2.3.1), the resistance is inversely proportional to *W* so that the maximization of the radiation efficiency of LIG antennas requires much larger traces ($W \geq 0.05\lambda$) than copper counterparts (Fig. 4b). Dipoles with shorter or larger lengths than the above optimal values will undergo a sensible degradation of performance. For example, dipoles shorter than $0.2\lambda$ would exhibit an efficiency less than 10%, independently (horizontal lines) on the width. This means that the size reduction of LIG antennas when required, would generate a not negligible degradation of gains. Moreover, conventional impedance matching techniques, adding distributed impedance to sub-resonant miniaturized antennas, namely, meandering, T-match, $\Gamma$-match, and Loop-match, are rather inefficient with LIG devices. Indeed, such configurations introduce differential current modes, namely mutually close currents of opposite

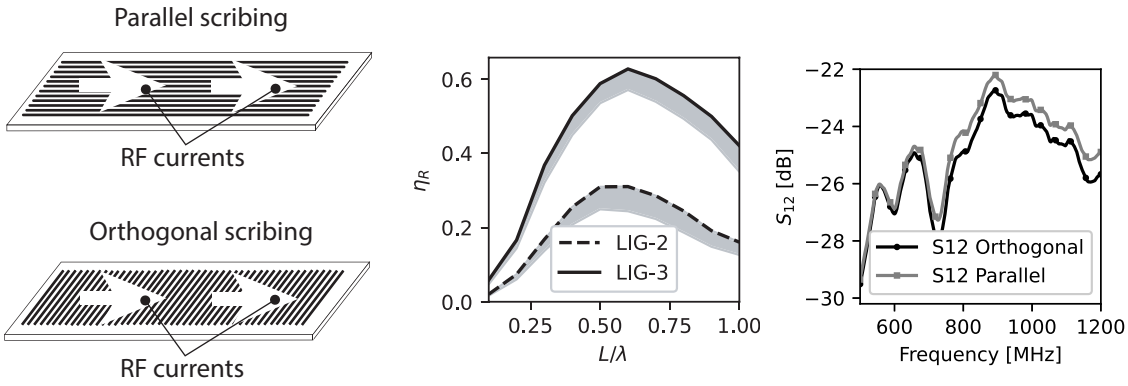


Fig. 5: (a) Surface anisotropy induced by the lasing direction. (b) Simulated decrement of radiation efficiency (gray zone) due to conductor's anisotropy, namely when the current flows in the orthogonal direction to the lasing groves. (c) Measured $S_{21}$ between two couples of identical $\lambda/4$ monopoles both considering parallel (gray square) and orthogonal (black dot) scribing and placed $30$ cm far from each other.

verse, that do not produce net radiation. While this effect is not particularly detrimental in the case of antennas made of good conductors, the modest conductivity of LIG trace generates instead a not negligible power loss that kills the antenna performance. A possible mean for miniaturization and matching is the use of lumped tuning inductors that avoid differential currents. However, the robust and reliable interconnection of Surface Mounting Devices (SMD) on LIG traces is still an open issue. Standard lead soldering is impractical, and the conductive epoxy adhesive is the only feasible alternative even though it does not provide robust adhesion or negligible contact resistance.

### 3.3. Effects of lasing rastering and anisotropy

Most of the commercially available laser engravers scribe the precursor following unidirectional rastering so that the surface finish of the graphene has a typical non-homogeneous appearance with parallel grooves. The electrical conductivity is hence anisotropic and depends on the direction of the surface currents w.r.t. the rastering pattern. When the current is forced to flow orthogonally to the LIG grooves, it degrades by a 25% [28], [82]. This reduction will in turn produce a further degradation of the radiation efficiency of the order of 0.5 dB (simulated results in Fig. 5a). The comparison between the measured $S_{21}$ of two couples of identical $\lambda/4$ monopoles both with parallel and orthogonal scribing corroborates the numerical results. Accordingly, the lasing patterning should match as well as possible the expected lead direction of the current flow on the antenna that could be preliminary predicted by simulations on a reference homogeneous conductor.

## 4. Integration

### 4.1. Soldering of electronics and connectors

As graphene is a semiconductor, standard lead soldering to interconnect discrete components and connectors is uneffective for LIG traces due to the lack of interfacial bonding metallic layer. Conductive epoxy glue, instead, is a suitable choice. A possible option is the CW2400 conductive epoxy from Chemtronics [83] having a volume resistivity lower than $10^{-3}\ \Omega/cm$. This adhesive can be even cured at room temperature for $24$ hours. However, to improve the conductivity, to minimize the additional losses and to increase the adhesion, the sample must be cured in a oven (from $60^{\circ}C$ to $80^{\circ}C$) for $5$ minutes.

### 4.2. Antenna-sensor integration

When the antenna is coupled with a low-frequency sensor, as in the case of interdigital capacitors (IDC) coated with a sensitive material, and in turn connected to a sampling ICs as in [84], [85], the presence of high-frequency electromagnetic fields generated during the communication link may produce artifacts in the measured sensor data. There are typically two effects related to the RF currents that are induced on the IDC by *(i)* the interrogating field and by *(ii)* the backscattering of the antenna. These currents may enter the analog port of the IC, produce artifacts in the measurements, and even generate an upset. Moreover, there

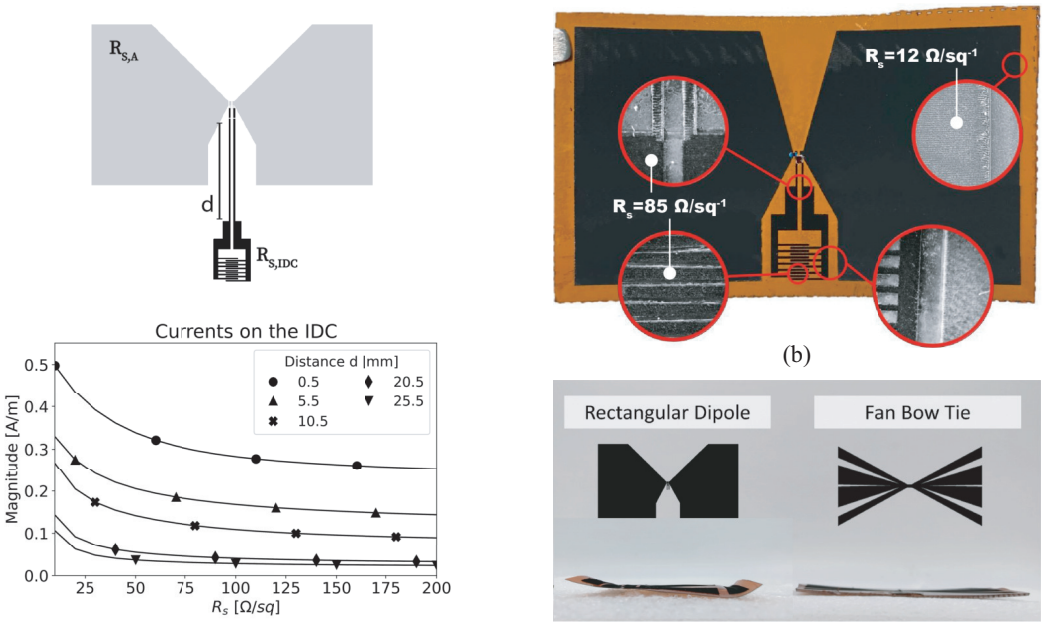


Fig. 6: (a) Antenna-sensor cohabitation: layout of a RFID wireless sensor with variable antenna-IDC distance and sheet resistance ($R_{S,IDC}$) on top and simulated average module of the RF currents on the IDC w.r.t. sensor distance and sheet resistance on the bottom. (b) Example of integration between a dipole antenna ($L = 70$ mm and $W = 40$ mm) and an IDC obtained with different laser settings. Details of macroscopic LIGs' morphologies in the insets. (c) Comparison between the thermal bending for the non-optimized and for the optimized dipole antenna layout.

could be parasitic capacitances between the antenna and the sensor itself if the latter is closely packed to the radiating element so that the measurement of the IDC capacitance is subjected to uncertainties.

LIG manufacturing offers unique degrees of freedom to get rid of the above problems without introducing additional choking devices thanks to the possibility to modulate the sheet resistance on the device. For this purpose, the antenna and the IDC can be manufactured, within a same lasing process, by exploiting different laser settings so that the sheet resistance of the antenna is miminized to improve the communication, while, the graphene of the IDC is produced with a higher resistance to act as an RF absorber. The resulting device is a hetero-structure with non-uniform resistance. For instance, Fig. 6a shows a bow-tie dipole connected to a IDC through a two-conductor transmission line. The parametric analysis of the average RF currents (@ 868 MHz) on the IDC region connected to a bow-tie dipole, when varying its sheet resistance and the length of the line, shows that a sheet resistance of the IDC higher that 75 $\Omega/sq$. significantly reduces the unwanted current on the IDC for any IDC-antenna distance. The resulting heterostructure is shown in Fig. 6b.

### *4.3. Reduction of thermal bending*

The high temperatures involved in the lasing process cause the precursor to bend and induce wrinkles on its surface. This phenomenon, which is particularly relevant for big lased areas, causes manufacturing imperfections during lasing since the correct focusing is not achieved all over the substrate and the resulting rastering may result in defects.

A possible countermeasure to mitigate thermal bending is to shape the layout of the antenna to minimize the lasing area while preserving the current paths of the original geometry [25]. Fig. 6c shows an example of a bow-tie dipole reshaping by resorting to a fan configuration where the width of the fingers was progressively reduced to mitigate thermal bending without significantly reducing the performance of the antenna. In particular, such a solution granted approximately the same radiation gain ($-9.5$ dBi) of the flat dipole antenna ($-9.3$ dBi) but with half of the lased area thus significantly reducing the deformation of the substrate.

TABLE III: AVERAGED PEAK AND TOTAL VARIATION OF SHEET RESISTANCE IN CASE OF PERIODIC BENDING, CONTACT WITH DRY AND WET OBJECTS.

| Configuration | Bending | | Dry object | | Wet object | |
|---|---|---|---|---|---|---|
| | $\Delta R_S^p$ [$\Omega/sq.$] | $\Delta R_S^T$ [$\Omega/sq.$] | $\Delta R_S^p$ [$\Omega/sq.$] | $\Delta R_S^T$ [$\Omega/sq.$] | $\Delta R_S^p$ [$\Omega/sq.$] | $\Delta R_S^T$ [$\Omega/sq.$] |
| **LIG-1** | $12.6 \pm 2.75$ | $-0.12 \pm 0.11$ | $-0.26 \pm 0.32$ | $0.04 \pm 0.03$ | $0.28 \pm 0.37$ | $0.40 \pm 0.07$ |
| **LIG-2** | $22.9 \pm 8.95$ | $0.06 \pm 0.17$ | $-12.7 \pm 2.97$ | $0.00 \pm 0.12$ | $-4.34 \pm 3.11$ | $0.23 \pm 0.17$ |
| **LIG-3** | $14.8 \pm 6.89$ | $0.03 \pm 0.08$ | $-0.25 \pm 0.52$ | $0.00 \pm 0.06$ | $-0.19 \pm 0.25$ | $0.07 \pm 0.12$ |

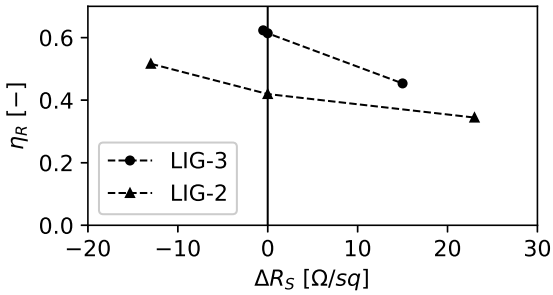


Fig. 7: Overall impact on the radiation efficiency at $868$ MHz of the external stimuli that modify the sheet resistance of a $L = 0.6\lambda$ and $W = 0.06\lambda$ dipole in case of two LIG materials.

## 5. Durability

Environmental agents, such as temperature or humidity gradients, and mechanical interactions with surrounding objects (e.g. bending and contact with dry and wet objects), especially in the case of IoT applications, may alter the electrical and durability features of LIG devices. The above effects can be quantitatively evaluated in the lab [60] by emulating periodic stress and by measuring the change of the sheet resistance against the stressful agents. In particular, the following two metrics can be considered: *i*) the average variation of sheet resistance during each periodic stimulus ($\Delta R_S^P$), and *ii*) the total difference between the sheet resistance after the application of each stimulus and the unperturbed one averaged by the number of cycles ($\Delta R_S^T$).

As a rule of thumb, the impact of mechanical stresses on LIG electrical properties is mainly controlled by the macroscopic morphology of the sample, while in the case of soft stimuli, such as temperature and humidity gradients, the microscopic/atomic structure prevails. As a matter of fact, bending, namely the more stressful agent, causes a nearly doubled variation of sheet resistance in the case of LIG-2, which is characterized by a fluffy morphology, w.r.t. other samples (Tab. III). LIG-3, which instead has a different atomic structure (Tab. I), exhibits an opposite behavior when exposed to variable environmental conditions.

The impact of the above variation of the sheet resistance on the radiation performance of LIG antennas is reported in Fig. 7 where the efficiency of the optimal-size dipoles at the typical frequencies of IoT applications (as in Tab. II) are simulated v.s. the variation of sheet resistance.

In the worst case, namely during the periodic bending, the degradation of performance becomes relevant when the sheet resistance increases by more than $10\ \Omega/sq.$ which corresponds to a reduction of the radiation efficiency of more than $20\%$ in the case of the most conductive material (LIG-3). Thus, depending on the specific application, a further margin has to be introduced in the link budget to account for possible detrimental effects during real-life service.

## 6. Summary and Conclusion

This paper addressed most of the relevant issues related to the design, manufacture, and testing of LIG antennas. Although several materials are reported to be used as precursor layers, PI is particularly convenient due to the large amount of carbon inside and, above all, for its availability in many sizes, thicknesses, and surface appearance (for instance adhesive).

The most relevant findings for the LIG on PI, that are useful to be accounted for by designers, are summarised next:

*i.* At radio-frequency, LIG must be considered as a two-dimensional conductor fully penetrable by an

impinging EM wave, and suitable to be simulated by the surface impedance with the Leontovich condition;

*ii.* Simulations and experiments indicate that there exists an optimal electrical size maximizing radiation gain regardless of the frequency of operation or lasing settings. These only affect the maximum achievable radiation efficiency, which is $4.5$ dB to $2$ dB less than that of equivalent copper antennas;

*iii.* The miniaturization of the antenna is particularly detrimental to the efficiency thus making the design of antennas in the sub-GHz range challenging;

*iv.* The direction of rastering during lasing is important since, in the case of engraving orthogonal to the natural flow of the currents, it can degrade the antenna performance of a further $0.5 - 1$ dB;

*v.* The involved high temperature of the manufacturing process induces an unwanted bending of the substrate potentially making the resulting graphene antenna non-homogeneous, especially for large areas. Thermal bending can be minimized by engineering the antenna layout to minimize the laser area without degrading the radiation performance;

*vi.* Electronic components and connectors can be interconnected to LIG traces by using conductive epoxy glue;

*vii.* LIG with reduced conductivity can be exploited when designing sensors connected to the antenna to naturally dump the currents induced by the external interrogating RF field;

*viii.* The impact of environmental gradients of temperature and humidity on the sheet resistance of LIG traces is not critical. Instead, in the case of hard stimuli (i.e., contact with dry or wet objects or bending), a further margin of $1$ dB in the link budget should be considered to account for a possible variation of the nominal value of sheet resistance during real-life applications.

Overall, antennas made by LIG are still in their infancy, and we expect further progress concerning the improvement of surface conductivity and the several possibilities offered by the lasing process. We expect further improvements by combining 3D printed substrates made by thermoplastic polymers, such as PEEK (Poly-Ether-Ether-Ketone), PES (Poly-Ether-Sulfone), PSU (Poly-Sulfone), and PP (Poly-Propylene) with laser engraving to generate more graphene and to hence lower the sheet resistance. These improvements hold potential for the eco-friendly and sustainable mass production of disposable and easily recyclable IoT devices of the near future.

## 7. Acknowledgments

Authors wish to thank Prof. Eugenio Martinelli and his collaborators dr. Joanna Filippi and dr. Gianni Antonelli, for discussions, suggestions and precious technical support.

## References

[1] J. Lin, Z. Peng, Y. Liu, F. Ruiz-Zepeda, R. Ye, E. L. Samuel, M. J. Yacaman, B. I. Yakobson, and J. M. Tour, "Laser-induced porous graphene films from commercial polymers," *Nature communications*, vol. 5, no. 1, p. 5714, 2014.

[2] A. F. Carvalho, A. J. Fernandes, C. Leitão, J. Deuermeier, A. C. Marques, R. Martins, E. Fortunato, and F. M. Costa, "Laser-induced graphene strain sensors produced by ultraviolet irradiation of polyimide," *Advanced Functional Materials*, vol. 28, no. 52, p. 1805271, 2018.

[3] S.-Y. Jeong, Y.-W. Ma, J.-U. Lee, G.-J. Je, and B.-s. Shin, "Flexible and highly sensitive strain sensor based on laser-induced graphene pattern fabricated by 355 nm pulsed laser," *Sensors*, vol. 19, no. 22, p. 4867, 2019.

[4] L. Huang, H. Wang, P. Wu, W. Huang, W. Gao, F. Fang, N. Cai, R. Chen, and Z. Zhu, "Wearable flexible strain sensor based on three-dimensional wavy laser-induced graphene and silicone rubber," *Sensors*, vol. 20, no. 15, p. 4266, 2020.

[5] B. Kulyk, B. F. Silva, A. F. Carvalho, S. Silvestre, A. J. Fernandes, R. Martins, E. Fortunato, and F. M. Costa, "Laser-induced graphene from paper for mechanical sensing," *ACS Applied Materials & Interfaces*, vol. 13, no. 8, pp. 10 210–10 221, 2021.

[6] D. Wu, Q. Peng, S. Wu, G. Wang, L. Deng, H. Tai, L. Wang, Y. Yang, L. Dong, Y. Zhao *et al.*, "A simple graphene nh3 gas sensor via laser direct writing," *Sensors*, vol. 18, no. 12, p. 4405, 2018.

[7] S.-Y. Xia, Y. Long, Z. Huang, Y. Zi, L.-Q. Tao, C.-H. Li, H. Sun, and J. Li, "Laser-induced graphene (lig)-based pressure sensor and triboelectric nanogenerator towards high-performance self-powered measurement-control combined system," *Nano Energy*, vol. 96, p. 107099, 2022.

[8] A. Kaidarova, N. Alsharif, B. N. M. Oliveira, M. Marengo, N. R. Geraldi, C. M. Duarte, and J. Kosel, "Laser-printed, flexible graphene pressure sensors," *Global Challenges*, vol. 4, no. 4, p. 2000001, 2020.

[9] M. G. Stanford, K. Yang, Y. Chyan, C. Kittrell, and J. M. Tour, "Laser-induced graphene for flexible and embeddable gas sensors," *ACS nano*, vol. 13, no. 3, pp. 3474–3482, 2019.

[10] F. Wang, K. Wang, B. Zheng, X. Dong, X. Mei, J. Lv, W. Duan, and W. Wang, "Laser-induced graphene: preparation, functionalization and applications," *Materials technology*, vol. 33, no. 5, pp. 340–356, 2018.

[11] M. Marengo, G. Marinaro, and J. Kosel, "Flexible temperature and flow sensor from laser-induced graphene," in *2017 IEEE SENSORS*. IEEE, 2017, pp. 1–3.

[12] S. Gandla, M. Naqi, M. Lee, J. J. Lee, Y. Won, P. Pujar, J. Kim, S. Lee, and S. Kim, "Highly linear and stable flexible temperature sensors based on laser-induced carbonization of polyimide substrates for personal mobile monitoring," *Advanced Materials Technologies*, vol. 5, no. 7, p. 2000014, 2020.
[13] S. Yin, H. Ibrahim, P. S. Schnable, M. J. Castellano, and L. Dong, "A field-deployable, wearable leaf sensor for continuous monitoring of vapor-pressure deficit," *Advanced Materials Technologies*, vol. 6, no. 6, p. 2001246, 2021.
[14] K. K. Adhikari, C. Wang, T. Qiang, and Q. Wu, "Polyimide-derived laser-induced porous graphene-incorporated microwave resonator for high-performance humidity sensing," *Applied Physics Express*, vol. 12, no. 10, p. 106501, 2019.
[15] X. Shi, F. Zhou, J. Peng, R. Wu, Z.-S. Wu, and X. Bao, "One-step scalable fabrication of graphene-integrated micro-supercapacitors with remarkable flexibility and exceptional performance uniformity," *Advanced Functional Materials*, vol. 29, no. 50, p. 1902860, 2019.
[16] A. Lamberti, F. Clerici, M. Fontana, and L. Scaltrito, "A highly stretchable supercapacitor using laser-induced graphene electrodes onto elastomeric substrate," *Advanced Energy Materials*, vol. 6, no. 10, p. 1600050, 2016.
[17] M. G. Stanford, J. T. Li, Y. Chyan, Z. Wang, W. Wang, and J. M. Tour, "Laser-induced graphene triboelectric nanogenerators," *ACS nano*, vol. 13, no. 6, pp. 7166–7174, 2019.
[18] M. R. Abdul-Aziz, S. A. Mohassieb, N. A. Eltresy, M. M. Yousef, B. Anis, S. O. Abdellatif, and A. S. Khalil, "Enhancing the performance of polygon monopole antenna using graphene/tmdcs heterostructures," *IEEE Transactions on Nanotechnology*, vol. 19, pp. 269–273, 2020.
[19] M. Ahmad, G. Cantarella, M. A. C. Angeli, M. Madagalam, C. Ebner, M. Ciocca, R. Riaz, P. Ibba, M. Petrelli, I. Merino *et al.*, "2.4 ghz microstrip patch antenna fabricated by means of laser induced graphitization of a cellulose-based paper substrate," in *2021 IEEE International Flexible Electronics Technology Conference (IFETC)*. IEEE, 2021, pp. 0044–0046.
[20] A. Sartanavičius, J. Žemgulytė, P. Ragulis, K. Ratautas, and R. Trusovas, "Laser-induced graphene in polyimide for antenna applications," *Crystals*, vol. 13, no. 7, p. 1003, 2023.
[21] B. Sindhu, A. Kothuru, P. Sahatiya, S. Goel, and S. Nandi, "Laser-induced graphene printed wearable flexible antenna-based strain sensor for wireless human motion monitoring," *IEEE Transactions on Electron Devices*, vol. 68, no. 7, pp. 3189–3194, 2021.
[22] A. Rivadeneyra, J. F. Salmeron, N. Rodriguez, D. P. Morales, R. Colella, F. P. Chietera, and L. Catarinucci, "Laser-fabricated antennas for rfid applications," in *2020 50th European Microwave Conference (EuMC)*. IEEE, 2021, pp. 812–815.
[23] F. P. Chietera, R. Colella, A. Verma, E. Ferraris, C. E. Corcione, C. L. Moraila-Martinez, D. Gerardo, Y. H. Acid, A. Rivadeneyra, and L. Catarinucci, "Laser-induced graphene, fused filament fabrication, and aerosol jet printing for realizing conductive elements of uhf rfid antennas," *IEEE Journal of Radio Frequency Identification*, vol. 6, pp. 601–609, 2022.
[24] A. Salvia, A. Mostaccio, G. Antonelli, E. Martinelli, and G. Marrocco, "Full-lig wireless batteryless sensor for the detection of amines," in *2023 IEEE International Conference on Flexible and Printable Sensors and Systems (FLEPS)*, 2023, pp. 1–4.
[25] A. Mostaccio, A. Salvia, G. Antonelli, E. Martinelli, and M. Gaetano, "Laser-induced graphene fan antenna for rfid applications," in *2023 IEEE 13th International Conference on RFID Technology and Applications (RFID-TA)*. IEEE, 2023.
[26] A. Mostaccio, A. Salvia, G. Antonelli, E. Martinelli, and G. Marrocco, "Upper bound performances of laser-induced graphene dipoles in the uhf band," in *2023 8th International Conference on Smart and Sustainable Technologies (SpliTech)*. IEEE, 2023, pp. 1–4.
[27] A. Mostaccio, G. Antonelli, C. Occhiuzzi, E. Martinelli, and G. Marrocco, "Experimental characterization of laser induced graphene (lig) antennas for s-band wearable applications in 5g," in *2022 IEEE 12th International Conference on RFID Technology and Applications (RFID-TA)*. IEEE, 2022, pp. 51–54.
[28] G. Karimi, I. Lau, M. Fowler, and M. Pope, "Parametric study of laser-induced graphene conductive traces and their application as flexible heaters," *International Journal of Energy Research*, vol. 45, no. 9, pp. 13 712–13 725, 2021.
[29] Y. Chyan, R. Ye, Y. Li, S. P. Singh, C. J. Arnusch, and J. M. Tour, "Laser-induced graphene by multiple lasing: toward electronics on cloth, paper, and food," *ACS nano*, vol. 12, no. 3, pp. 2176–2183, 2018.
[30] M. Tavakkoli Gilavan, M. S. Rahman, A. Minhas-Khan, S. Nambi, and G. Grau, "One-step fabrication of low-resistance conductors on 3d-printed structures by laser-induced graphene," *ACS Applied Electronic Materials*, vol. 3, no. 9, pp. 3867–3875, 2021.
[31] H. Wang, H. Wang, Y. Wang, X. Su, C. Wang, M. Zhang, M. Jian, K. Xia, X. Liang, H. Lu *et al.*, "Laser writing of janus graphene/kevlar textile for intelligent protective clothing," *ACS nano*, vol. 14, no. 3, pp. 3219–3226, 2020.
[32] S. Zhu, Z. Lei, Y. Dou, C.-W. Lou, J.-H. Lin, and J. Li, "Sputter-deposited nickel nanoparticles on kevlar fabrics with laser-induced graphene for efficient solar evaporation," *Chemical Engineering Journal*, vol. 452, p. 139403, 2023.
[33] W. Yang, W. Zhao, Q. Li, H. Li, Y. Wang, Y. Li, and G. Wang, "Fabrication of smart components by 3d printing and laser-scribing technologies," *ACS applied materials & interfaces*, vol. 12, no. 3, pp. 3928–3935, 2019.
[34] J. Wang, N. Wang, D. Xu, L. Tang, and B. Sheng, "Flexible humidity sensors composed with electrodes of laser induced graphene and sputtered sensitive films derived from poly (ether-ether-ketone)," *Sensors and Actuators B: Chemical*, vol. 375, p. 132846, 2023.
[35] A. K. Thakur, H. Mahbub, F. H. Nowrin, and M. Malmali, "Highly robust laser-induced graphene (lig) ultrafiltration membrane with a stable microporous structure," *ACS applied materials & interfaces*, vol. 14, no. 41, pp. 46 884–46 895, 2022.
[36] B. A. Getachew, D. S. Bergsman, and J. C. Grossman, "Laser-induced graphene from polyimide and polyethersulfone precursors as a sensing electrode in anodic stripping voltammetry," *ACS Applied Materials & Interfaces*, vol. 12, no. 43, pp. 48 511–48 517, 2020.

[37] C. H. Dreimol, H. Guo, M. Ritter, T. Keplinger, Y. Ding, R. Günther, E. Poloni, I. Burgert, and G. Panzarasa, "Sustainable wood electronics by iron-catalyzed laser-induced graphitization for large-scale applications," *Nature communications*, vol. 13, no. 1, p. 3680, 2022.
[38] C. Qu, M. Lu, Z. Zhang, S. Chen, D. Liu, D. Zhang, J. Wang, and B. Sheng, "Flexible microstructured capacitive pressure sensors using laser engraving and graphitization from natural wood," *Molecules*, vol. 28, no. 14, p. 5339, 2023.
[39] R. Ye, Y. Chyan, J. Zhang, Y. Li, X. Han, C. Kittrell, and J. M. Tour, "Laser-induced graphene formation on wood," *Advanced Materials*, vol. 29, no. 37, p. 1702211, 2017.
[40] Y. Wang, Z. Niu, J. Chen, Y. Zhai, Y. Xu, and S. Luo, "Freestanding laser induced graphene paper based liquid sensors," *Carbon*, vol. 153, pp. 472–480, 2019.
[41] Z. Li, L. Lu, Y. Xie, W. Wang, Z. Lin, B. Tang, and N. Lin, "Preparation of laser-induced graphene fabric from silk and its application examples for flexible sensor," *Advanced Engineering Materials*, vol. 23, no. 9, p. 2100195, 2021.
[42] Y. Guo, C. Zhang, Y. Chen, and Z. Nie, "Research progress on the preparation and applications of laser-induced graphene technology," *Nanomaterials*, vol. 12, no. 14, p. 2336, 2022.
[43] M. Liu, J. Wu, and H. Cheng, "Effects of laser processing parameters on properties of laser-induced graphene by irradiating co2 laser on polyimide," *Science China Technological Sciences*, vol. 65, no. 1, pp. 41–52, 2022.
[44] Y. Chen, J. Long, S. Zhou, D. Shi, Y. Huang, X. Chen, J. Gao, N. Zhao, and C.-P. Wong, "Uv laser-induced polyimide-to-graphene conversion: modeling, fabrication, and application," *Small Methods*, vol. 3, no. 10, p. 1900208, 2019.
[45] A. Minhas-Khan, S. Nambi, and G. Grau, "Low-resistance laser-induced graphitic carbon by maximizing energy delivery and pulse overlap," *Carbon*, vol. 181, pp. 310–322, 2021.
[46] Q. Li, T. Wu, W. Zhao, J. Ji, and G. Wang, "Laser-induced corrugated graphene films for integrated multimodal sensors," *ACS Applied Materials & Interfaces*, vol. 13, no. 31, pp. 37 433–37 444, 2021.
[47] A. Vashisth, M. Kowalik, J. C. Gerringer, C. Ashraf, A. C. Van Duin, and M. J. Green, "Reaxff simulations of laser-induced graphene (lig) formation for multifunctional polymer nanocomposites," *ACS Applied Nano Materials*, vol. 3, no. 2, pp. 1881–1890, 2020.
[48] A. Lamberti, M. Serrapede, G. Ferraro, M. Fontana, F. Perrucci, S. Bianco, A. Chiolerio, and S. Bocchini, "All-speek flexible supercapacitor exploiting laser-induced graphenization," *2D Materials*, vol. 4, no. 3, p. 035012, 2017.
[49] X. Sun, X. Liu, and F. Li, "Sulfur-doped laser-induced graphene derived from polyethersulfone and lignin hybrid for all-solid-state supercapacitor," *Applied Surface Science*, vol. 551, p. 149438, 2021.
[50] S. Baachaoui, W. Mabrouk, A. Rabti, O. Ghodbane, and N. Raouafi, "Laser-induced graphene electrodes scribed onto novel carbon black-doped polyethersulfone membranes for flexible high-performance microsupercapacitors," *Journal of Colloid and Interface Science*, vol. 646, pp. 1–10, 2023.
[51] N. H. Barbhuiya, A. Kumar, and S. P. Singh, "A journey of laser-induced graphene in water treatment," *Transactions of the Indian National Academy of Engineering*, vol. 6, pp. 159–171, 2021.
[52] S. P. Singh, Y. Li, J. Zhang, J. M. Tour, and C. J. Arnusch, "Sulfur-doped laser-induced porous graphene derived from polysulfone-class polymers and membranes," *ACS nano*, vol. 12, no. 1, pp. 289–297, 2018.
[53] A. Z. Yazdi, I. O. Navas, A. Abouelmagd, and U. Sundararaj, "Direct creation of highly conductive laser-induced graphene nanocomposites from polymer blends," *Macromolecular Rapid Communications*, vol. 38, no. 17, p. 1700176, 2017.
[54] A. K. Thakur, B. Lin, F. H. Nowrin, and M. Malmali, "Comparing structure and sorption characteristics of laser-induced graphene (lig) from various polymeric substrates," *ACS ES&T Water*, vol. 2, no. 1, pp. 75–87, 2021.
[55] Dupont, "Kapton® hn general-purpose polyimide film," https://www.dupont.com/electronics-industrial/kapton-hn.html, 2023.
[56] McMaster-Carr, "Polyimide sheets," https://www.mcmaster.com/products/polyimide-sheets, 2023.
[57] A. Kaidarova and J. Kosel, "Physical sensors based on laser-induced graphene: A review," *IEEE Sensors Journal*, vol. 21, no. 11, pp. 12 426–12 443, 2020.
[58] L. Wang, Z. Wang, A. N. Bakhtiyari, and H. Zheng, "A comparative study of laser-induced graphene by co2 infrared laser and 355 nm ultraviolet (uv) laser," *Micromachines*, vol. 11, no. 12, p. 1094, 2020.
[59] L. Cheng, W. Guo, X. Cao, Y. Dou, L. Huang, Y. Song, J. Su, Z. Zeng, and R. Ye, "Laser-induced graphene for environmental applications: progress and opportunities," *Materials Chemistry Frontiers*, vol. 5, no. 13, pp. 4874–4891, 2021.
[60] A. Mostaccio, G. Antonelli, M. Bragaglia, E. Martinelli, and G. Marrocco, "Comparative evaluation of laser induced graphene (lig) traces on polyimide under soft and hard stress for iot applications," *IEEE Journal on Flexible Electronics*, 2023.
[61] T.-S. D. Le, H.-P. Phan, S. Kwon, S. Park, Y. Jung, J. Min, B. J. Chun, H. Yoon, S. H. Ko, S.-W. Kim *et al.*, "Recent advances in laser-induced graphene: Mechanism, fabrication, properties, and applications in flexible electronics," *Advanced Functional Materials*, vol. 32, no. 48, p. 2205158, 2022.
[62] B. D. Abera, I. Ortiz-Gómez, B. Shkodra, F. J. Romero, G. Cantarella, L. Petti, A. Salinas-Castillo, P. Lugli, and A. Rivadeneyra, "Laser-induced graphene electrodes modified with a molecularly imprinted polymer for detection of tetracycline in milk and meat," *Sensors*, vol. 22, no. 1, p. 269, 2021.
[63] Y. Li, D. X. Luong, J. Zhang, Y. R. Tarkunde, C. Kittrell, F. Sargunaraj, Y. Ji, C. J. Arnusch, and J. M. Tour, "Laser-induced graphene in controlled atmospheres: from superhydrophilic to superhydrophobic surfaces," *Advanced Materials*, vol. 29, no. 27, p. 1700496, 2017.
[64] Y. Wang, G. Wang, M. He, F. Liu, M. Han, T. Tang, and S. Luo, "Multifunctional laser-induced graphene papers with combined defocusing and grafting processes for patternable and continuously tunable wettability from superlyophilicity to superlyophobicity," *Small*, vol. 17, no. 42, p. 2103322, 2021.
[65] M. Naftaly, S. Das, J. Gallop, K. Pan, F. Alkhalil, D. Kariyapperuma, S. Constant, C. Ramsdale, and L. Hao, "Sheet resistance measurements of conductive thin films: a comparison of techniques," *Electronics*, vol. 10, no. 8, p. 960, 2021.

[66] D.-W. Wang, M.-J. Yuan, J.-Y. Dai, and W.-S. Zhao, "Electrical modeling and characterization of graphene-based on-chip spiral inductors," *Micromachines*, vol. 13, no. 11, p. 1829, 2022.
[67] J. Kang, Y. Matsumoto, X. Li, J. Jiang, X. Xie, K. Kawamoto, M. Kenmoku, J. H. Chu, W. Liu, J. Mao *et al.*, "On-chip intercalated-graphene inductors for next-generation radio frequency electronics," *Nature Electronics*, vol. 1, no. 1, pp. 46–51, 2018.
[68] R. Wang, S. Raju, M. Chan, and L. J. Jiang, "Low frequency behavior of cvd graphene from dc to 40 ghz," *Progress In Electromagnetics Research C*, vol. 71, pp. 1–7, 2017.
[69] N. D'Agati and J. Zec, "Laser-scribed graphene (lsg) fabrication method for microwave circuit applications," *IEEE Microwave and Wireless Components Letters*, vol. 31, no. 11, pp. 1215–1218, 2021.
[70] S. Russo, M. Craciun, M. Yamamoto, A. Morpurgo, and S. Tarucha, "Contact resistance in graphene-based devices," *Physica E: Low-dimensional Systems and Nanostructures*, vol. 42, no. 4, pp. 677–679, 2010.
[71] G. Reeves and H. Harrison, "Obtaining the specific contact resistance from transmission line model measurements," *IEEE Electron device letters*, vol. 3, no. 5, pp. 111–113, 1982.
[72] J. S. Gomez-Diaz, J. Perruisseau-Carrier, P. Sharma, and A. Ionescu, "Non-contact characterization of graphene surface impedance at micro and millimeter waves," *Journal of Applied Physics*, vol. 111, no. 11, 2012.
[73] F. Majeed, T. Fickenscher, M. Shahpari, and D. V. Thiel, "Measurement of surface conductivity of graphene at w-band," *Microwave and Optical Technology Letters*, vol. 61, no. 7, pp. 1747–1754, 2019.
[74] X.-C. Wang, A. Díaz-Rubio, and S. A. Tretyakov, "An accurate method for measuring the sheet impedance of thin conductive films at microwave and millimeter-wave frequencies," *IEEE Transactions on Microwave Theory and Techniques*, vol. 65, no. 12, pp. 5009–5018, 2017.
[75] M. Ye, R. U. Tariq, X.-L. Zhao, W.-D. Li, and Y.-N. He, "Contactless measurement of sheet resistance of nanomaterial using waveguide reflection method," *Materials*, vol. 13, no. 22, p. 5240, 2020.
[76] M. Liang, M. Tuo, S. Li, Q. Zhu, and H. Xin, "Graphene conductivity characterization at microwave and thz frequency," in *The 8th European Conference on Antennas and Propagation (EuCAP 2014)*. IEEE, 2014, pp. 489–491.
[77] L. Hao, J. Gallop, S. Goniszewski, O. Shaforost, N. Klein, and R. Yakimova, "Non-contact method for measurement of the microwave conductivity of graphene," *Applied Physics Letters*, vol. 103, no. 12, 2013.
[78] H.-J. Lee, E. Kim, J.-G. Yook, and J. Jung, "Intrinsic characteristics of transmission line of graphenes at microwave frequencies," *Applied Physics Letters*, vol. 100, no. 22, 2012.
[79] O. Niksan, B. C. Wyatt, K. K. Kazemi, B. Anasori, and M. H. Zarifi, "Mxene free standing films: Unlocking the impact of flake sizes in microwave resonant structures in humid environments," *Small*, p. 2300848, 2023.
[80] Y. Houeix, F. Romero, D. Morales, N. Rodriguez, and D. Kaddour, "Novel frequency selective surface made of laser-induced graphene," in *2023 IEEE 13th International Conference on RFID Technology and Applications (RFID-TA)*. IEEE, 2023.
[81] S. Amendola and G. Marrocco, "Optimal performance of epidermal antennas for uhf radio frequency identification and sensing," *IEEE Transactions on Antennas and Propagation*, vol. 65, no. 2, pp. 473–481, 2016.
[82] B. Chen, Z. T. Johnson, D. Sanborn, R. G. Hjort, N. T. Garland, R. R. Soares, B. Van Belle, N. Jared, J. Li, D. Jing *et al.*, "Tuning the structure, conductivity, and wettability of laser-induced graphene for multiplexed open microfluidic environmental biosensing and energy storage devices," *ACS nano*, vol. 16, no. 1, pp. 15–28, 2021.
[83] Chemtronics, "Circuitworks conductive epoxy," https://www.chemtronics.com/circuitworks-conductive-epoxy-2, 2023.
[84] S. Tedjini, G. Andia-Vera, M. Zurita, R. C. Freire, and Y. Duroc, "Augmented rfid tags," in *2016 IEEE Topical Conference on Wireless Sensors and Sensor Networks (WiSNet)*. IEEE, 2016, pp. 67–70.
[85] J. Fernández-Salmerón, A. Rivadeneyra, F. Martínez-Martí, L. F. Capitán-Vallvey, A. J. Palma, and M. A. Carvajal, "Passive uhf rfid tag with multiple sensing capabilities," *Sensors*, vol. 15, no. 10, pp. 26 769–26 782, 2015.
[86] C. Lv, C. Hu, J. Luo, S. Liu, Y. Qiao, Z. Zhang, J. Song, Y. Shi, J. Cai, and A. Watanabe, "Recent advances in graphene-based humidity sensors," *Nanomaterials*, vol. 9, no. 3, p. 422, 2019.
[87] R. Liang, A. Luo, Z. Zhang, Z. Li, C. Han, and W. Wu, "Research progress of graphene-based flexible humidity sensor," *Sensors*, vol. 20, no. 19, p. 5601, 2020.
[88] H. Kun, L. Bin, M. Orban, Q. Donghai, and Y. Hongbo, "Accurate flexible temperature sensor based on laser-induced graphene material," *Shock and Vibration*, vol. 2021, pp. 1–7, 2021.
[89] M.-C. Chen, C.-L. Hsu, and T.-J. Hsueh, "Fabrication of humidity sensor based on bilayer graphene," *IEEE Electron Device Letters*, vol. 35, no. 5, pp. 590–592, 2014.
[90] J. Wu, Z. Wu, K. Tao, C. Liu, B.-R. Yang, X. Xie, and X. Lu, "Rapid-response, reversible and flexible humidity sensing platform using a hydrophobic and porous substrate," *Journal of Materials Chemistry B*, vol. 7, no. 12, pp. 2063–2073, 2019.
[91] A. D. Smith, K. Elgammal, F. Niklaus, A. Delin, A. C. Fischer, S. Vaziri, F. Forsberg, M. Råsander, H. Hugosson, L. Bergqvist *et al.*, "Resistive graphene humidity sensors with rapid and direct electrical readout," *Nanoscale*, vol. 7, no. 45, pp. 19 099–19 109, 2015.
[92] C. Miozzi, F. Amato, and G. Marrocco, "Performance and durability of thread antennas as stretchable epidermal uhf rfid tags," *IEEE Journal of Radio Frequency Identification*, vol. 4, no. 4, pp. 398–405, 2020.
[93] N. Dalal, Y. Gu, D. R. Hines, A. Dasgupta, and S. Das, "Cracks in the 3d-printed conductive traces of silver nanoparticle ink," *Journal of Micromechanics and Microengineering*, vol. 29, no. 9, p. 097001, 2019.
[94] L. Huang, Y. Liu, G. Li, Y. Song, J. Su, L. Cheng, W. Guo, G. Zhao, H. Shen, Z. Yan *et al.*, "Ultrasensitive, fast-responsive, directional airflow sensing by bioinspired suspended graphene fibers," *Nano Letters*, vol. 23, no. 2, pp. 597–605, 2023.

**Gaetano Marrocco** (Senior Member, IEEE) is Full Professor of Electromagnetics Engineering at the University of Roma Tor Vergata, where he currently leads the Medical Engineering School. Since 2002, he has been a pioneer in Radiofrequency Identification and Sensing. His current research focuses on wireless-activated sensors, Wearable and Epidermal Electronics, and structural antennas for sensorized skins, smart prostheses, and finger augmentation devices for Tactile Internet. He serves as an Associate Editor of the IEEE Journal of Radiofrequency Identification and track Editor of the IEEE Journal of Flexible Electronics. Additionally, he chairs the Italian Section of URSI Commission D Electronics and Photonics and is a co-founder and president of the University spin-off RADIO6ENSE. RADIO6ENSE is actively involved in short-range electromagnetic sensing for Industrial Internet of Things, Smart Manufacturing, Automotive, and Digital Health. He is also listed in the PLOS 2022 ranking of the Top 2 % Scientists Worldwide.

**Alessio Mostaccio** (Student Member, IEEE) Alessio Mostaccio received the MSc in Medical Engineering (Hons.) in 2021 from the University of Rome Tor Vergata, Italy, where he is currently pursuing his PhD. He is also a part-time employee in the RADIO6ENSE Srl company. His research is focused on laser-induced graphene (LIG) for designing and manufacturing antennas starting from polymeric precursors. He is also focused on researching and developing biocompatible RFID-based methods to monitor food quality. He has been a co-author of the paper ”Cyber-tooth: Antennified dental Implant for RFID Wireless temperature Monitoring” winner of the Best Student Paper Award at the 2021 IEEE International Conference on RFID Technology and Applications (RFID-TA). He secured the 2nd place at the Student Best Paper Award competition at the 2023 IEEE International Conference on Flexible, Printable Sensors and Systems (IEEE FLEPS).